RSC Advances

PAPER

View Article Online
View Journal | View Issue

Cite this: *RSC Adv.*, 2017, **7**, 1905

Chelation assisted exfoliation of layered borides towards synthesizing boron based nanosheets†

Asha Liza James and Kabeer Jasuja*

The ability to exfoliate tightly bound layered ionic solids has vastly expanded the realm of 2D materials beyond graphene. A crucial step in such exfoliation strategies involves extraction of the inter-planar atoms holding the layers together. Here we present a chelation assisted selective extraction strategy for exfoliating layered metal borides, a family of layered ionic solids that are isostructural to intercalated graphite, with metal atoms sandwiched between graphenic planes of boron. We present evidence for the exfoliation of two metal borides, namely magnesium diboride and aluminium diboride, into aqueous dispersions of few-layer-thick boron based nanosheets, by employing chelation assisted targeted extraction of the inter gallery metal atoms. Chemical analysis of the nanosheets reveals a substantial loss of metal atoms and the presence of boron-planes decorated with hydride, hydroxyl, and oxy-functional groups that are likely derived from the aqueous milieu. The nanosheets exhibit a distinct crumpled morphology with micron-scale lateral dimensions and few layer thickness. These functionalized nanosheets derived from metal borides present promising platforms to leverage the potential of nanoscaled boron. The soft chemical exfoliation approach demonstrated here achieves delamination in a single step under ambient conditions without any additional aides like sonication and holds immense prospects for exfoliating a host of 3D precursors.

Received 11th November 2016
Accepted 18th December 2016

DOI: 10.1039/c6ra26658d

www.rsc.org/advances

Introduction

The current decade is witness to the horizon of two-dimensional (2D) materials expanding beyond graphene and its analogs derived from weakly bonded van der Waals solids.[1,2] Layered ionic solids, with much stronger interlayer bonding, are being intently probed by scientists for exfoliation in order to enable the prospective confinement of newer compounds to two dimensionality.[3] This has been best exemplified by the recent discovery of MXenes (quasi 2D transition metal carbides and/or nitrides),[4] obtained by exfoliating layered $M_{n+1}AX_n$ compounds or MAX phases; where M is an early transition metal (Ti, V, Nb, Ta), A is an A-group element (Al, Si, Sn, In), X is carbon and/or nitrogen, and n ranges from 1–3.[5] MAX phases embody a combination of metallic, covalent, and ionic bonds that hold together $M_{n+1}X_n$ layers interleaved with atoms of A-group element.[6] Naguib *et al.* have demonstrated that exfoliation of such complex layered compounds can be realized by selectively etching the A atoms (that are relatively less tightly bound), weakening the layered structure that subsequently delaminates to yield quasi 2D layers referred as MXenes.[7,8] Such selective extraction approaches have also been used earlier to exfoliate other layered ionic solids such as perovskites, oxides, and hydroxides of transition/rare earth metals.[9] In these approaches, the cations/anions spaced in between the charged 2D metal oxide/hydroxide polyhedral layers are exchanged with bulky organic counter ions to enable delamination.[3] $CaSi_2$ is yet another layered ionic solid that was reported (as early as 2006) to have been chemically exfoliated into single crystal oxy-functionalized silicon nanosheets by selective extraction of Ca ions using propylamine hydrochloride.[10] Significant efforts, both experimental and theoretical,[11] have been devoted to explore the possibility of two dimensionality in more such complex layered materials which offer diverse composition, tuneable chemistry, and a richer palette of physico-chemical properties.[12–14]

A layered ionic solid that presents an intriguing case in the pursuit of two dimensionality beyond graphene is magnesium diboride (MgB_2), a compound that rose to fame in 2001 owing to its superconducting properties.[15] This layered compound has covalently bonded hexagonal networks of boron (similar to the carbon honeycomb planes in graphene) alternated with layers of magnesium atoms, the Mg–B bond being predominantly ionic (structure of the compound is represented in Fig. S0 in ESI†).[16,17] Such a layered constitution offers MgB_2 an extremely promising attribute: its prospective exfoliation can facilitate an

Discipline of Chemical Engineering, Indian Institute of Technology Gandhinagar, Gujarat 382355, India. E-mail: kabeer@iitgn.ac.in

† Electronic supplementary information (ESI) available: TEM, HRTEM, and FESEM images of nanosheets derived from MgB_2 and AlB_2, thickness distribution from AFM, FESEM-EDX data, details on ICP-AES calculations, Raman spectra, XPS spectra, UV-Vis spectra of the nanosheet dispersions, SAED patterns, XRD patterns of the nanosheets, Zeta Potential data, XRD and FESEM data of the chelant treated boride powders. See DOI: 10.1039/c6ra26658d

access to quasi-planar forms of boron. This capability is immensely significant in view of the range of curious properties hosted by boron—high melting point, low density yet high hardness, high Young's modulus, and remarkable opto-electronic properties.[18] Congeneric to graphene, the quasi-planar forms of boron are expected to help utilize these rich properties to their true potential. In fact, several theoretical studies have explored the prospects offered by 2D forms of boron.[19,20] For example, Zhang *et al.*, determined the diverse structures possible and preferred for 2D boron on metal substrates.[21] However, their physical realization had remained largely elusive[22] until 2015, when successful bottom-up synthesis of boron nanosheets was reported by Xu *et al.*[23] and others.[24–27] While such bottom-up approaches are gradually evolving, the top-down exfoliative synthesis of 2D sheets of boron has remained unexplored, mainly due to the apparent absence of a suitable layered parent material. MgB_2 presents an apt layered boron based compound to address this missing link. Moreover, MgB_2 is the flagship compound of a whole family of metal borides, which offer interesting properties—mechanical hardness, superconductivity, thermoelectric and magnetic behaviours owing to the interplay between the covalent B framework and metal lattice.[28] Delamination of metal borides could thus yield newer quasi 2D materials with an array of potentially useful properties. In light of these prospects, there have indeed been theoretical pursuits to examine the thinning down of MgB_2 into 2D sheets.[29–31]

Recently, we have realized the delamination of MgB_2 by utilizing the exfoliative ability of ultrasonication.[32] We had made a specific observation that the nanosheets obtained were Mg-deficient, indicating that the displacement of Mg atoms loosens the bulk boride crystals and enables their exfoliation into few-layer-thick nanosheets. This observation prompted us to develop an alternative strategy, designed to purposely extract the inter layer magnesium atoms selectively, and thereby assist in the exfoliation of MgB_2. A suitable means for achieving this objective is to sequester the Mg ions using an appropriate chelating agent. Ethylene diamine tetraacetic acid (EDTA) is a versatile chelant, well known for its high affinity sequestering of Mg^{2+} ions.[33] To the best of our knowledge, a top down approach employing chelation has not yet been adopted as a stand-alone tool towards exfoliating layered 3D materials.

In this article, we report a soft chemical approach that utilizes the phenomenon of chelation to exfoliate layered metal borides into boron based nanosheets. We first show that an aqueous solution of disodium EDTA (Na_2EDTA) molecules can extract a significant fraction of the interlayer Mg atoms from the MgB_2 crystals leading to their exfoliation into few-layer-thick nanosheets deficient in Mg. The loss of Mg atoms is observed to be compensated by acquiring functional groups from the aqueous environment. The nanosheets are well dispersed in water and found to be decorated with hydride, hydroxyl, and oxy-functional groups that impart an overall negative charge to these nanosheets. We also show that a similar strategy can be successfully extended to AlB_2, resulting in nanosheets with a markedly metal (Al) deficient stoichiometry compared to the nanosheets exfoliated from MgB_2. In both cases, the chelation assisted targeted extraction of the inter gallery metal atoms leads to exfoliation of the boride crystals without the need to effect delamination by any conventional means like sonication or shearing.

Experimental

Synthesis of nanosheets

Briefly, 0.46 g of magnesium diboride powder (−100 mesh size, Sigma Aldrich, 99% purity) was added to 100 ml of 0.1 M disodium ethylene diamine tetra acetate dihydrate (>99%, Fluka) solution in deionized water (1 : 1 molar ratio) and magnetically stirred for an hour, inside a fume hood. The temperature was maintained at ~20 °C during the reaction. A black coloured opaque solution was obtained with vigorous evolution of gas, forming a froth layer at the top. The solution was left undisturbed for a day, the ambient temperatures being around 25 °C, upon which black solids sediment leaving a clear yellow solution. The top part of the solution was subjected to two rounds of centrifugation at 1500 rpm for 45 minutes to settle unexfoliated particles. The final supernatant was collected and dialyzed against cold deionized water (maintained at temperature of ~10 °C), using cellulosic dialysis sacks (21 mm diameter, 12 kDa molecular weight cut off, Sigma) for ~30 hours. The dialyzed sample was clear and colourless; it was collected and stored for further analysis. This sample exhibited a strong Tyndall effect upon shining a laser beam through it, confirming it to be a colloidal dispersion. A part of it was subjected to lyophilization for 48 hours, resulting in a pale white, fluffy structure. The above steps are depicted in Fig. 1. The same procedure was adopted for exfoliating AlB_2, wherein aluminium diboride powder (−325 mesh, Sigma Aldrich) was used.

Structural characterization

TEM imaging was performed using Philips Tecnai 20 TEM, operated at 200 kV. HRTEM images were acquired on a JEOL JEM 2100, operated at 200 kV. The colloidal dispersion was deposited onto lacey carbon copper grids (Ted Pella, 300 mesh), dried under ambient conditions and used for imaging. FE-SEM analysis was performed on JEOL JSM-7600F operated at 5–10 kV. The lyophilized nanosheets powder was dusted onto conducting carbon tape fixed on stubs and was sputter coated by platinum prior to imaging. AFM imaging was done on Bruker Multimode-8-AM in ScanAsyst tapping mode. Samples for AFM were prepared by re-dispersing the lyophilized nanosheet powder in DI water and spin coating ~70 μl of this dispersion onto a freshly cleaved mica substrate (3000 rpm, 60 seconds). The XRD analysis was performed on a diffractometer from Bruker AXS, Germany (D8 Discover).

Chemical characterization

ICP-AES studies were carried out to measure concentration of the elements in the samples on a Perkin Elmer ICP-OES Spectrometer Optima 3300 RL. Ten ml of the dialyzed nanosheets dispersion was analysed against a control of Ultrapure Millipore water (Type I). FTIR spectroscopy was undertaken to

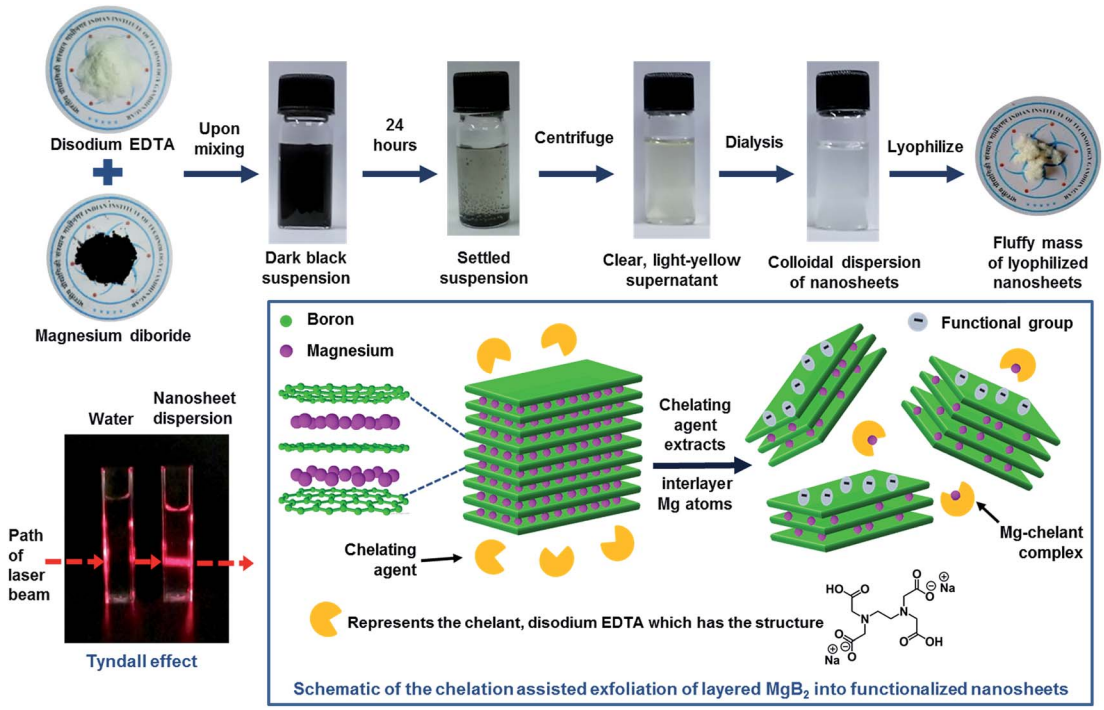

Fig. 1 Chelation assisted exfoliation of magnesium diboride: top panel presents a graphical summary of the experimental route to realize the exfoliation of bulk MgB_2 using chelation. Tyndall effect shown by the dialyzed sample indicates it to be a colloidal dispersion. The schematic in the box depicts EDTA molecules chelating a substantial fraction of the interlayer Mg atoms, assisting the delamination of parent MgB_2 crystal into few-layer-thick, Mg deficient nanosheets that acquire functional groups from the aqueous ambience.

qualitatively understand the chemical make-up of the nanosheets. IR spectra were recorded for standard MgB_2, lyophilized nanosheets powder and lyophilized supernatant powder (mixed with KBr and made into pellets) on a Perkin Elmer Spectrum GX spectrometer. For standard AlB_2 and the lyophilized powder of nanosheets derived from AlB_2 (mixed with KBr and made into pellets), the IR spectra were recorded on a Thermo Scientific Nicolet iS10 FTIR spectrometer. ^{11}B solid state NMR spectroscopy experiments were performed on a JEOL ACX 400 MHz spectrometer with 9.4 T magnet, equipped with a 2.5 mm magic angle spinning (MAS) probe operated at 25 kHz. The spectral frequency for ^{11}B was 128.284 MHz and the chemical shifts were referenced with external standard as sodium borohydride which has a 42.06 ppm chemical shift relative to the primary standard, $F_3B{\cdot}O(C_2H_5)_2$. The spectrum was acquired in a single pulse experiment. The data was smoothened using FFT filters in Origin software. Raman spectroscopy was performed with a 785 nm laser source using Renishaw inVia Raman microscope. About 5 mg of lyophilized nanosheet powder and standard MgB_2 powder were used. The noise in the data was corrected by using FFT filters in the Origin graphing and data analysis software. X-ray photoelectron spectroscopy (Axis Ultra, Kratos Analytical, Shimadzu, employing monochromatic Al Kα X-ray radiation of $h\nu = 1486.6$ eV) was performed to chemically characterize the sample. The 1s spectra of B, Mg, and O were acquired. Standard MgB_2 was analysed as a pellet, while the nanosheets sample was drop-casted on a silica wafer and the dried wafer was analysed. Zeta potential analyses of the aqueous dispersions of MgB_2 and AlB_2 derived nanosheets were performed on a Malvern Zetasizer Nano ZS.

Results and discussion

Fig. 1 represents a graphical summary of the chelation assisted exfoliation route, illustrating that a selective extraction of the Mg atoms by the chelant molecules can result in the delamination of the parent boride crystal. As shown in the top panel, the supernatant, recovered after the chemical exfoliation route, was dialyzed against cold water to remove the Mg–EDTA complex and any residual chelant molecules, so as to "clean" the sample. This dialyzed sample was then lyophilized to obtain the nanosheets in a powder-form as a fluffy mass with a yield of ~7.2%. The Tyndall effect shown by the dialyzed sample, as shown in Fig. 1, indicates it to be a colloidal dispersion.

Transmission electron microscopy (TEM) analysis of the colloidal dispersion was carried out to characterize the dispersed phase. Fig. 2 presents TEM images depicting sheet-like nanostructures with lateral dimensions ranging from ~500 nm to few micrometers. Most nanosheets exhibit a distinct crumpled appearance, some seem to have few to several folds, wrinkles, and appear to curl up at the edges (Fig. 2a–c). Some nanosheets also exhibit globular structures on their surfaces (Fig. 2d). The presence of folds, crumples, and wrinkles in nanosheets exfoliated from MgB_2 were also reported in our previous work where we linked their origin to several factors ranging from capillary effects during sample deposition

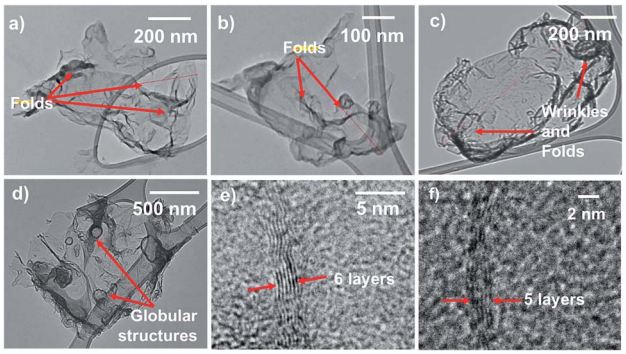

Fig. 2 TEM images showing crumpled morphology and HRTEM images showing 'few layer thickness' of the nanosheets: (a–c) nanosheets exhibiting folds, crumples, wrinkles, and curled edges; (d) nanosheets showing globular structures on their surface; (e and f) transverse view of folds in the nanosheets under HRTEM showing them to be made of 5–6 layers.

to functional group induced stress on the nanosheet backbone.[32] Studies have reported that flat, unsupported graphene sheets tend to become more unstable as their lateral dimensions increase, leading to folding or scrolling of the structures.[34,35] In addition, as explained further in the chemical analysis, the varying degrees of functionalization on these nanosheets could possibly result in hydrophobic pockets that get buried within these crumples so as to minimize the surface in contact with water. More TEM images of nanosheets exhibiting moderate to high crumpling can be found in the ESI Fig. S1 and S2.†

HRTEM images reveal that these nanosheets are few-layer-thick. Fig. 2e and f show high-resolution transverse views of folded edges of nanosheets, comprising ~5–6 layers. Similar images representing few-layer-thick nanosheets are included in the ESI Fig. S3 and S4.† EDX spectra were acquired under the TEM, as depicted in Fig. S3,† showing these are boron based materials. The presence of few-layer-thick nanosheets in the dispersion affirms that chelation has indeed facilitated the exfoliation of a layered ionic solid without requiring a supplementary aid such as sonication, as often is the case in liquid-phase exfoliation approaches.[36]

The thickness of nanosheets was obtained by atomic force microscopy (AFM) measurements. Fig. 3a shows an AFM scan and height profiles of the nanostructures spin coated on a mica substrate. Most of the nanosheets exhibit a thickness in the range of ~1.0–1.7 nm indicating their quasi two-dimensionality.

FE-SEM images of the lyophilized powder also show the presence of sheet like structures, as can be observed from Fig. 3b and c (also see Fig. S6 in ESI†). Some such structures are found to exhibit distinct perforations on their surfaces as shown in Fig. 4a and b and S7 in ESI.† Some nanosheets observed under AFM are also found to be perforated (Fig. 4c).

These perforations seem to be an outcome of the localized degradation of exfoliated MgB_2 under the low-pressure conditions during lyophilization, explained as follows. Bulk MgB_2 is known to mildly react with water that leads to surface degradation and release of gaseous boranes.[37,38] The exfoliated MgB_2 nanosheets present a much higher interfacial area that could enable a more pronounced reaction with water. A similar degradation of phosphorene nanosheets in aqueous environment has also been reported by Hanlon *et al.* in their study on liquid exfoliation of black phosphorous.[39] The vigorous gas evolution observed upon mixing the chelant and MgB_2 during the synthesis step can also be explained in this regard; the chelant treatment in aqueous medium could have enhanced the reaction of MgB_2 with water resulting in the evolution of gaseous borane derivatives.

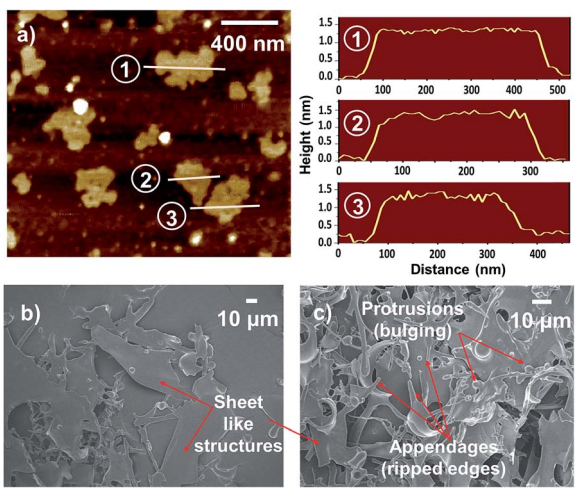

Fig. 3 AFM and FE-SEM images: (a) AFM scan with corresponding height profiles depicting few layer thick nanosheets having ~1.0–1.7 nm thickness; (b and c) FE-SEM images reveal the lamellar nature of the lyophilized sample along with rod like appendages and spherical protrusions.

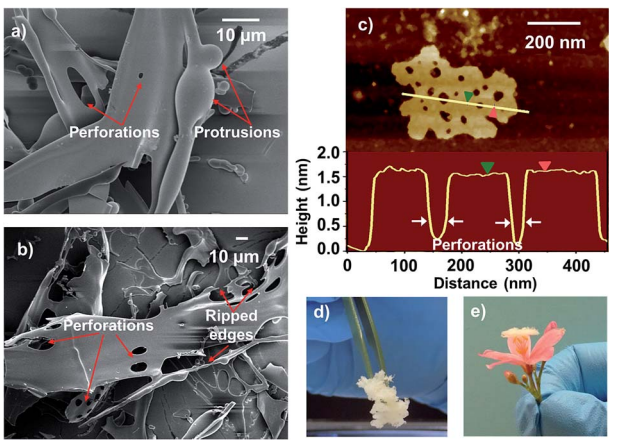

Fig. 4 Perforations in lyophilized form of nanosheets: (a and b) FE-SEM images depicting perforations (likely caused by the evolution of gases as a result of exfoliated nanosheet–water reactions) and spherical protrusions (likely caused by subsequent bulging); (c) AFM image depicting a "holey" nanosheet, with the corresponding height profile; (d and e) photographs of the fluffy mass obtained upon lyophilizing the nanosheets solution; the presence of perforations in nanosheets result in a fluffy mass, which is very light in weight.

The gas evolved as a result of exfoliated MgB_2 nanosheet–water interactions could lead to local spherical protrusions, which can rupture under low-pressure conditions (while freeze-drying) leading to perforations. This is supported by the presence of spherical protrusions and rod-like appendages as depicted in Fig. 3b and c and S7a and b (in ESI†). While the gas evolution leads to bulging and inflated structures (spherical protrusions), their puncture leads to perforations and tearing of the nanostructures (ripped edges) that manifest as appendages. The presence of perforations and fragmentations resulting from the *in situ* gas evolution, renders the lyophilized powder a light weight, porous, and fluffy architecture (as depicted in Fig. 4d and e), similar to the leavening strategy described by Niu *et al.* for r-GO foams.[40] Further experiments are underway to obtain a deeper understanding of these phenomena. Such an *in situ* gas evolution could offer possibilities towards 3D macroporous or mesoporous assemblies from these nanosheets, as has been the case with porous graphene materials.[41]

Selective extraction of the interlayer Mg atoms was confirmed by inductively coupled plasma atomic emission spectroscopy (ICP-AES) analysis of the dialyzed dispersion, which also validates the presence of boron based materials in the dispersion. Four different batches of nanosheet dispersions were analysed for their Mg and B content. The results presented in Table 1 indicate that as compared to the Mg : B ratio of 0.98 : 2 in standard MgB_2, the nanosheets exhibit an Mg-deficient stoichiometry (sample calculations can be found in ESI†). The loss of Mg atoms is also evidenced by the XPS results as discussed later. Further analysis of the nanosheets by FTIR suggests that the loss of a significant fraction of Mg atoms is compensated by acquiring functional groups from the aqueous environment. The Mg deficiency and extensive oxy-functionalization is also evident from the EDX spectra collected for the nanosheets under FE-SEM (Fig. S8 and S9 in ESI†); a comparison between standard MgB_2 and the nanosheets conveying the change in chemical composition has been graphically represented in Fig. S8 in the ESI.†

FTIR spectra were recorded for the lyophilized powder sample and standard MgB_2 powder, and compared for gaining insights into the chemical characteristics of the nanosheets (Fig. 5a). The FTIR spectrum of nanosheets indicates several new bands representing the presence of new functional groups acquired during exfoliation. The broad band observed in the range 3000–3500 cm^{-1} corresponds to the B–OH stretching mode and indicates possible hydroxyl functionalization.[42–44] The band at ~1118 cm^{-1} can also be attributed to the presence of B–OH functional groups as the B–OH in-plane bending is usually observed to be around 1000–1300 cm^{-1}.[45] The standard MgB_2 sample also displays bands corresponding to OH stretching at ~3400 cm^{-1} and water bending at ~1620 cm^{-1}, which are indicative of adsorbed moisture.[46] This is expected as MgB_2 is known to be hygroscopic.[47]

The nanosheets sample also exhibits a moderate band at ~2485 cm^{-1}, likely due to B–H stretching.[48] The strong band observed at 1585 cm^{-1} can be ascribed to hydrogen motions in B–H–B bridge.[43,44] These observations indicate the presence of hydride functionalities on the boron lattice. ^{11}B solid state NMR spectroscopy of the lyophilized nanosheets sample also revealed the presence of complex borohydride species (Fig. S10 in ESI†).[49,50] Strong absorption in the range of ~1310–1350 cm^{-1} is characteristic of B–O stretch and hence the band at 1326 cm^{-1} can be assigned to the presence of oxy-functional groups on boron lattice.[43] Also, the 1300–1450 cm^{-1} region has been linked to the asymmetric stretching of B–O in trigonal BO_3 and therefore the band near ~1407 cm^{-1} and the shoulder at ~1450 cm^{-1} can be attributed to higher oxides of boron.[51,52] Summing up, the FTIR results reveal that the nanosheets carry hydride, hydroxyl, and oxy-functionalities. These functional groups are likely acquired from the aqueous milieu in order to compensate for the loss of Mg atoms. Similar aqueous environment derived functionalization has been observed in the exfoliative synthesis of MXenes and silicon nanosheets.[4,10]

The presence of B–B bonds in the nanosheets was confirmed by Raman spectroscopy (shown in ESI Fig. S11†), as the B–B in-plane stretching gives rise to the characteristic E_{2g} vibrational phonon mode, typically observed in the range of ~550–650 cm^{-1}.[53] Comparison of the Raman spectra from standard MgB_2 and nanosheets also revealed that the oxy-functional groups have induced some disorder in the boron planes in the nanosheets; this is reflected in the Raman spectrum from the nanosheets as: (i) a shift in the in-plane vibrational E_{2g} phonon frequencies, and (ii) an additional peak near 751 cm^{-1} linked to the phonon density of states due to disorder.[54,55]

The nature of functional groups decorating the nanosheets was further analysed by X-ray photoelectron spectroscopy (XPS). B 1s spectrum from the standard MgB_2 sample (Fig. 5b) exhibits a primary peak at 188.3 eV and a secondary peak at 192.6 eV, in agreement with the available literature on MgB_2.[47] The primary peak is characteristic of the metal boride family as their binding energies range from ~187.2–188.5 eV.[56] The secondary peak is attributed to the presence of B_2O_3, commonly associated with bulk MgB_2 due to surface oxidation.[57–59] The B 1s spectrum of nanosheets is observed to be shifted to higher binding energies (in comparison to the characteristic metal boride peak) and is found to be composed of three daughter spectra upon deconvolution as shown in Fig. 5b inset. The daughter peak which contributes most significantly to the B 1s signal is centred at 191.9 eV, and is ascribed to the B–O bond indicating the

Table 1 ICP-AES analysis of nanosheet dispersions: the values suggest that chelation extracts a significant fraction of the interlayer Mg, resulting in the nanosheets having a Mg-deficient stoichiometry compared to bulk MgB_2 that has Mg : B ratio of 0.98 : 2[a]

	ICP-AES value (mg l^{-1})		Stoichiometric ratio
Sample	Mg	B	Mg : B
1	32.225	55.075	0.52 : 2
2	26.360	43.582	0.54 : 2
3	28.395	50.213	0.51 : 2
4	25.069	46.189	0.48 : 2

[a] Mg : B ratio in bulk MgB_2 is 0.98 : 2 as obtained from XRD analysis; the data is provided in ESI.

presence of oxidized boron atoms.[60,61] The two minor daughter peaks, centred at 193.2 eV and 194.4 eV, are designated to the higher oxides of boron,[62] the former being characteristic of B_2O_3.[63]

Mg 1s spectra (as shown in ESI Fig. S12†) indicate a significant reduction in the amount of Mg in the nanosheets in line with the ICP-AES results, confirming the selective extraction of Mg atoms. We also obtained valuable clues on the charge state of Mg atoms that remain integrated within the exfoliated nanosheets. It is known that in bulk MgB_2, while the Mg atoms donate their electrons to boron layers, there is also a back transfer of electrons from B to Mg^{2+} (as explained excellently by Talapatra and co-workers[57]) that reduces the formal charge on Mg to <2+. Thus, the Mg atoms in bulk MgB_2 are partially ionized and their binding energy is lesser than that corresponding to Mg^{2+}. We found that the Mg 1s spectrum from nanosheets shifts to a higher binding energy (1306.05 eV that corresponds to Mg^{2+}) as compared to the parent boride (1304.25 eV). An increase in the formal charge on Mg in the nanosheets is anticipated, as the oxy-functionalized boron planes are likely to act more electronegative towards Mg than bare boron planes. The higher binding energy of Mg atoms in nanosheets also suggests that they are held more strongly by the functionalized planes; this explains why some Mg atoms remain integrated within the nanosheets even after prolonged exposure to chelation. Further investigations are needed to understand the exact role of residual Mg atoms.

The heavy oxy-functionalization as evidenced by the XPS results renders excellent water dispersibility to the nanosheets and properties markedly different from parent MgB_2. The aqueous dispersion of nanosheets is completely transparent to the naked eye with a high absorbance in the UV regime (as shown in the optical spectrum in Fig. S13, ESI†). Also, the nanosheets exhibit an amorphous nature, which is expected due to the loss of Mg and functionalization (suggested by the SAED patterns shown in Fig. S14, ESI†). Such a "lack of crystallinity" of nanosheets has also been reported by Daeneke *et al.* in their report of reductive exfoliation of MoS_2 using hydrazine salts, into sub stoichiometric bilayers with lattice distortion.[64] 2D oxides obtained through a thermal annealing route from hydrous chlorides, exhibiting similar amorphous nature were also reported by Zhao *et al.*[65] This observation further corroborates the Raman spectroscopy results that indicate disorder in the lattice due to functional groups in the nanosheets. High resolution imaging under TEM also revealed the presence of defects and distortions in the lattice, with partly preserved hexagonal lattice regions (as shown in ESI Fig. S15†).

In order to ascertain that chelation has indeed extracted the Mg atoms from the inter gallery space as Mg–EDTA complex, thereby resulting in exfoliation, the Mg species present in the supernatant after the MgB_2–aqueous EDTA reaction, were characterized by performing FTIR analysis of the lyophilized form of this supernatant (ESI Fig. S17†). The peaks in the FTIR spectrum consist jointly of those originating from the boron based nanosheets as well as the Mg–EDTA complex. Peaks corresponding to $Na_2MgY{\cdot}4H_2O$ (where Y is ethylenediaminetetraacetate anion) as reported by Sawyer and Paulsen in their study on alkaline earth chelates of EDTA, could be seen in the spectrum.[66] They reported the following IR peaks for the $Na_2MgY{\cdot}4H_2O$ complex: 2920 cm^{-1} (–CH_2), 1610 cm^{-1} (–COO–), 1425 cm^{-1} (–COO–), and 1115 cm^{-1} (–C–N). It can be seen that the FTIR spectrum of the lyophilized supernatant also has similar peaks, indicating the presence of Mg–EDTA. Also, the band at 2800–3000 cm^{-1} corresponds to C–H stretching in the –CH_2 of EDTA; the acid form and sodium salts of EDTA show this peak in the region 3020–3030 cm^{-1}. It is reported that the aforementioned peak appearing between 2900 and 2950 cm^{-1} is a strong evidence for chelate formation.[67] Hence the peaks corresponding to EDTA in the supernatant sample are confirmed to originate from the Mg–EDTA chelation complex. As explained earlier in the FTIR analysis of the lyophilized nanosheets powder, peaks corresponding to hydroxyl, hydride, oxy functionalities on the nanosheets can be identified in this sample as well.

The successful exfoliation of MgB_2 by chelation assisted selective extraction inspired us to extend this approach to aluminium diboride (AlB_2), another member of the layered metal boride family. We found that a similar experimental

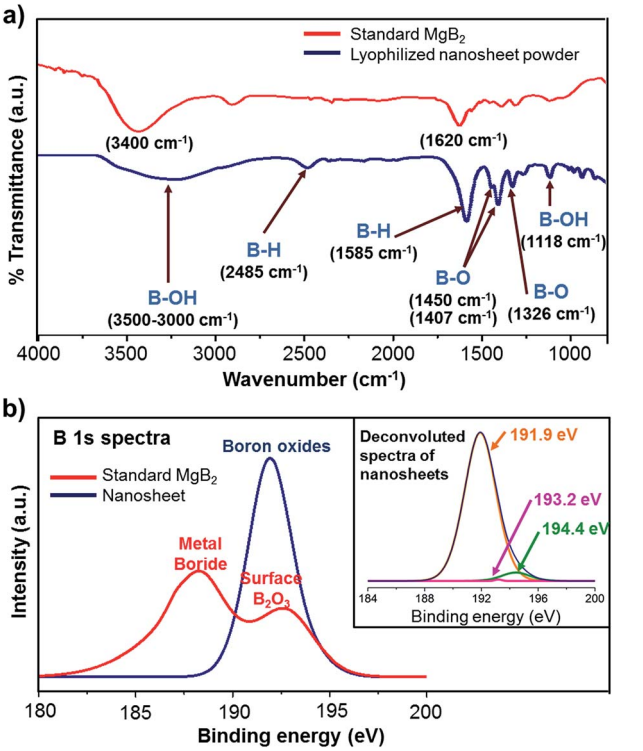

Fig. 5 Chemical analysis of the nanosheets: (a) FTIR spectra of standard MgB_2 and nanosheets are compared, indicating that the nanosheets are decorated with hydrides, hydroxides, and oxides; (b) B 1s spectrum from the XPS analysis shows that the chemical identity of the material shifts from that of a metal boride to oxy-functionalized boron upon exfoliation. MgB_2 displays a primary peak (188.3 eV) characteristic of the metal borides along with a secondary peak (192.6 eV) corresponding to the surface boron oxide layer. The nanosheets show an intense peak (191.9 eV), which is deconvoluted to three daughter spectra as shown in the inset, which correspond to higher oxides of boron.

methodology is effective in achieving exfoliation of AlB_2 as well into aqueous dispersions of boron based nanosheets. The nanosheets exhibit lateral dimensions > 1 μm, extremely crumpled morphologies, and few layer thickness as revealed by TEM and HRTEM images (Fig. 6a–c, ESI S18 and S19†). Lyophilizing the nanosheet dispersions gave a whitish powder with yields of ~4%. FE-SEM images of the lyophilized nanosheets sample show sheet like structures agglomerated together into bunches, as evident from Fig. 6d and ESI S20.† Typical perforated structures were not observed during FE-SEM imaging probably because, unlike in the case of MgB_2, the synthesis of AlB_2 derived nanosheets was not associated with vigorous gas evolution. FTIR analysis (Fig. 6f) indicates that the AlB_2 derived nanosheets are also functionalized with hydride, hydroxyl, and oxy groups, similar to their MgB_2 derived counterparts. Owing to this, the aqueous dispersions of these nanosheets are transparent and their optical spectrum shows high UV absorbance (ESI Fig. S23†).

We made an important observation that the AlB_2 derived nanosheets exhibit an even smaller metal atom : boron (Al : B) stoichiometric ratio as compared to MgB_2 derived nanosheets (Fig. 6e; see ESI† for ICP-AES calculations). A much higher degree of inter layer metal extraction from AlB_2 compared to MgB_2 crystals can be explained by the higher stability constant of Al–EDTA ($\log K = 16.3$) that is about twice that of Mg–EDTA ($\log K = 8.7$).[33] Another pertinent point is the nature of metal–B bond: the Al–B bond has a higher covalent bond energy (−1182 meV) when compared to the Mg–B bond (−1003 meV).[68] Thus, despite the presence of stronger metal–boron bonds in AlB_2, the higher affinity of the EDTA molecules for the Al atoms make them much more susceptible for selective extraction from the inter gallery space by chelation. These observations suggest the opportunities available for regulating the metal:boron stoichiometries by modulating chelant-interlayer metal affinities in further studies on exfoliation of metal borides. This ability confers chelation assisted selective extraction an added merit that apart from enabling exfoliation, it can also be tuned to obtain distinct variants of nanosheets from similar parent materials.

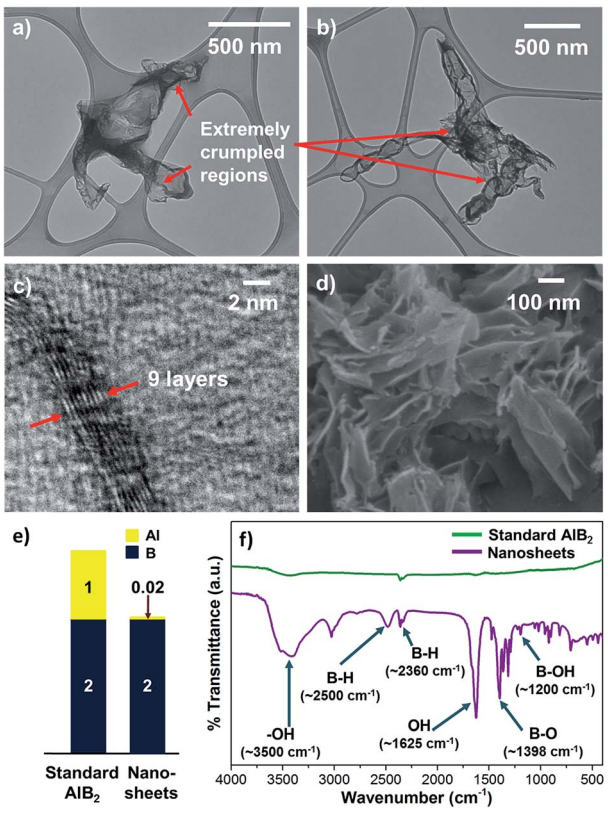

Fig. 6 Chelation assisted exfoliation of aluminium diboride: (a and b) TEM images showing the extremely crumpled morphology of the nanosheets; (c) HRTEM image of the transverse view of an edge of a nanosheet, indicating its few layer thickness; (d) FE-SEM image of the lyophilized nanosheets sample; (e) ICP-AES analysis reveals that these sheets are very rich in boron due to highly efficient removal of Al by Na_2EDTA; (f) FTIR spectra comparing the standard AlB_2 powder and the nanosheets.

Another interesting observation was made upon performing the zeta potential studies for understanding the colloidal stability of the nanosheet dispersions. It was found that the zeta potential values of nanosheet dispersions derived from AlB_2 were almost two-fold higher than those from MgB_2 (Fig. S24 in ESI†). It is possible that the very high levels of inter-gallery Al extraction has made the Al-deficient nanosheets much more prone to functionalization, thus imparting them with higher levels of colloidal stability.

In order to further understand how the chelating agents effect exfoliation of the borides by metal extraction, we attempted to characterize the chelant treated MgB_2 and AlB_2 powders for changes in their structure and morphology by XRD and FE-SEM (Fig. S25–S28 in Section IV of ESI†).[69] As compared to the standard MgB_2 and AlB_2 powders, the treated boride crystals show interlayer excavations that indicate removal of metal atoms by the chelating action of EDTA. The XRD results provide further evidence for the chemical exfoliation of metal borides due to chelation assisted extraction of interlayer Mg. XRD patterns for the MgB_2 and AlB_2 derived nanosheets are also included in the ESI (Fig. S16 and S21† respectively). As a control experiment, we also analysed supernatants from simple mixing of MgB_2 and water for the presence of any nanosheet like structures under TEM; the images as presented in ESI Fig. S29† reveal micron sized spherical and fused particles and hence eliminate the possibility that simple mixing in water could enable the dispersion of any nanosheets from the bulk material. Hence, it is indeed the chelating action of the EDTA molecules towards the interlayer metal atoms that is enabling the exfoliation of boride crystals.

The work reported here brings forth a compelling evidence for the potential of chelation assisted selective extraction strategy in exfoliating layered ionic compounds. The selective removal of the inter gallery metal atoms by the chelating agent leads to exfoliation of the parent boride crystals in a single step, without requiring any additional delamination events like sonication or shearing. This method adds onto the spectrum of selective extraction strategies being intensively researched in recent times for 2D material synthesis by providing a simple yet powerful targeted approach for interlayer atom removal

resulting in exfoliation. We anticipate that this liquid phase exfoliation technique can similarly be extended to a whole array of layered compounds which host interlayer metal atoms that can be targeted for selective extraction by chelation. The work reported here is the first top down approach that has availed the possibilities presented by chelation assisted selective extraction in realizing boron based nanosheets from the exfoliation of layered metal borides, providing fresh perspectives to nano dimensional boron science.

Conclusions

We have shown that chelation can be utilized as a stand-alone tool to exfoliate MgB_2, a layered ionic solid, to produce few-layer-thick boron based nanosheets. The implications of this ability go far beyond the present study as chelation assisted exfoliation can not only be extended to members of the metal boride family, as described for the case of AlB_2, but also other layered ionic solids such as metal oxides, metal carbides, and silicides having interlayer metal atoms that might be susceptible to chelation. This prospect is supplemented by an entire arsenal of chemical ligands that not only enable chelation but also assist in stabilization. Moreover, the presence of water-derived surface functional groups on nanosheets in the present study suggests the possibility of generating tailored interfaces by varying the nature of solvation. The porous, lamellar nature of the lyophilized nanosheets and the presence of B–H surface functionalities are expected to have important implications in evaluating the candidature of these nanomaterials for hydrogen storage, considering that boron compounds, especially borohydrides, are high potential materials for hydrogen storage.[70] These Mg-deficient and Al-deficient nanosheets are also promising building blocks to develop nanostructured electrodes in rechargeable Mg and Al ion batteries. Similar nanostructured materials are indeed being intensely researched and developed towards applications in such multivalent ion batteries; MXenes, for example, have shown promise as high performance battery materials with unique potential for Mg and Al ion storage.[71] Though applications in hydrogen storage and battery electrodes are theoretically predicted for boron based 2D materials,[19] several other avenues to leverage these uniquely functionalized boron planes could be uncovered upon further elucidation of the properties of these nanosheets. We anticipate that the exfoliation approach shown here can provide an additional impetus to the recent advances in realizing boron based two-dimensional materials and open up newer avenues to utilize their rich chemistry.

Acknowledgements

We are thankful to Vikas Patel (SICART, Anand, India), Reneesh B. and Anu A. S. (IIUCNN, Mahatma Gandhi University, Kottayam, India) for help with TEM and HRTEM imaging; Bhavin Kansara (IISER Mohali, India) for Raman spectroscopy and Sarath S. (ACNSMM, Kochi, India) for XPS analysis. We thank NMR Research Center, IISc Bangalore for solid state NMR spectroscopy. We are deeply grateful to IIT Gandhinagar Central Research Facility and would like to appreciate the help extended by Awaneesh Upadhyay and Vikram Karde (with FESEM); Tvarit Patel, Chetan Singh, Suganya Arumugam, and Narendra Bandaru (with AFM); Komal Pandey, Sophia Varghese, and Sanat Maiti (with XRD). We also thank Anuj Bisht for support with the FTIR analysis, and Seema Negi for help with Zeta Potential measurements. The work was supported by seed funding from IIT Gandhinagar; Fast Track Research Grant for Young Scientists (SB/FTP/ETA-114/2013) by Science and Engineering Research Board, Department of Science and Technology, India; and INSPIRE Faculty Award Research Grant (DST/INSPIRE/04/2014/001601) by the Department of Science and Technology, India.

Notes and references

1 A. C. Ferrari, F. Bonaccorso, V. Fal'ko, K. S. Novoselov, S. Roche, P. Boggild, S. Borini, F. H. L. Koppens, V. Palermo, N. Pugno, J. A. Garrido, R. Sordan, A. Bianco, L. Ballerini, M. Prato, E. Lidorikis, J. Kivioja, C. Marinelli, T. Ryhanen, A. Morpurgo, J. N. Coleman, V. Nicolosi, L. Colombo, A. Fert, M. Garcia-Hernandez, A. Bachtold, G. F. Schneider, F. Guinea, C. Dekker, M. Barbone, Z. Sun, C. Galiotis, A. N. Grigorenko, G. Konstantatos, A. Kis, M. Katsnelson, L. Vandersypen, A. Loiseau, V. Morandi, D. Neumaier, E. Treossi, V. Pellegrini, M. Polini, A. Tredicucci, G. M. Williams, B. Hee Hong, J.-H. Ahn, J. Min Kim, H. Zirath, B. J. van Wees, H. van der Zant, L. Occhipinti, A. Di Matteo, I. A. Kinloch, T. Seyller, E. Quesnel, X. Feng, K. Teo, N. Rupesinghe, P. Hakonen, S. R. T. Neil, Q. Tannock, T. Lofwander and J. Kinaret, *Nanoscale*, 2015, **7**, 4598–4810.

2 F. Schwierz, J. Pezoldt and R. Granzner, *Nanoscale*, 2015, **7**, 8261–8283.

3 S. Z. Butler, S. M. Hollen, L. Cao, Y. Cui, J. A. Gupta, H. R. Gutiérrez, T. F. Heinz, S. S. Hong, J. Huang, A. F. Ismach, E. Johnston-Halperin, M. Kuno, V. V. Plashnitsa, R. D. Robinson, R. S. Ruoff, S. Salahuddin, J. Shan, L. Shi, M. G. Spencer, M. Terrones, W. Windl and J. E. Goldberger, *ACS Nano*, 2013, **7**, 2898–2926.

4 M. Naguib, O. Mashtalir, J. Carle, V. Presser, J. Lu, L. Hultman, Y. Gogotsi and M. W. Barsoum, *ACS Nano*, 2012, **6**, 1322–1331.

5 P. Eklund, M. Beckers, U. Jansson, H. Högberg and L. Hultman, *Thin Solid Films*, 2010, **518**, 1851–1878.

6 Z. M. Sun, *Int. Mater. Rev.*, 2011, **56**, 143–166.

7 M. Naguib, M. Kurtoglu, V. Presser, J. Lu, J. Niu, M. Heon, L. Hultman, Y. Gogotsi and M. W. Barsoum, *Adv. Mater.*, 2011, **23**, 4248–4253.

8 M. Naguib, V. N. Mochalin, M. W. Barsoum and Y. Gogotsi, *Adv. Mater.*, 2014, **26**, 992–1005.

9 M. Osada and T. Sasaki, *J. Mater. Chem.*, 2009, **19**, 2503–2511.

10 H. Nakano, T. Mitsuoka, M. Harada, K. Horibuchi, H. Nozaki, N. Takahashi, T. Nonaka, Y. Seno and H. Nakamura, *Angew. Chem., Int. Ed.*, 2006, **45**, 6303–6306.

11 Q. Tang, Z. Zhou and Z. Chen, *Wiley Interdiscip. Rev.: Comput. Mol. Sci.*, 2015, **5**, 360–379.
12 R. Ma and T. Sasaki, *Acc. Chem. Res.*, 2015, **48**, 136–143.
13 A. Gupta, T. Sakthivel and S. Seal, *Prog. Mater. Sci.*, 2015, **73**, 44–126.
14 M. Naguib and Y. Gogotsi, *Acc. Chem. Res.*, 2015, **48**, 128–135.
15 J. Nagamatsu, N. Nakagawa, T. Muranaka, Y. Zenitani and J. Akimitsu, *Nature*, 2001, **410**, 63–64.
16 F. R. Wagner, A. I. Baranov, Y. Grin and M. Kohout, *Z. Anorg. Allg. Chem.*, 2013, **639**, 2025–2035.
17 P. de la Mora, M. Castro and G. Tavizon, *J. Solid State Chem.*, 2002, **169**, 168–175.
18 C. Amartya, M. K. Lauren, J. K. Kate, A. M. John and S. H. Narayan, in *Boron Science*, CRC Press, 2011, DOI: 10.1201/b11199–27.
19 X.-B. Li, S.-Y. Xie, H. Zheng, W. Q. Tian and H.-B. Sun, *Nanoscale*, 2015, **7**, 18863–18871.
20 E. S. Penev, S. Bhowmick, A. Sadrzadeh and B. I. Yakobson, *Nano Lett.*, 2012, **12**, 2441–2445.
21 Z. Zhang, Y. Yang, G. Gao and B. I. Yakobson, *Angew. Chem., Int. Ed.*, 2015, **54**, 13022–13026.
22 Y. Liu, E. S. Penev and B. I. Yakobson, *Angew. Chem.*, 2013, **125**, 3238–3241.
23 J. Xu, Y. Chang, L. Gan, Y. Ma and T. Zhai, *Adv. Sci.*, 2015, **2**, 1500023.
24 R. B. Patel, T. Chou and Z. Iqbal, *J. Nanomater.*, 2015, **2015**, 7.
25 G. Tai, T. Hu, Y. Zhou, X. Wang, J. Kong, T. Zeng, Y. You and Q. Wang, *Angew. Chem., Int. Ed.*, 2015, **54**, 15473–15477.
26 A. J. Mannix, X.-F. Zhou, B. Kiraly, J. D. Wood, D. Alducin, B. D. Myers, X. Liu, B. L. Fisher, U. Santiago, J. R. Guest, M. J. Yacaman, A. Ponce, A. R. Oganov, M. C. Hersam and N. P. Guisinger, *Science*, 2015, **350**, 1513–1516.
27 B. Feng, J. Zhang, Q. Zhong, W. Li, S. Li, H. Li, P. Cheng, S. Meng, L. Chen and K. Wu, *Nat. Chem.*, 2016, **8**, 563–568.
28 S. Carenco, D. Portehault, C. Boissière, N. Mézailles and C. Sanchez, *Chem. Rev.*, 2013, **113**, 7981–8065.
29 Y. Zhao, C. Ban, Q. Xu, S.-H. Wei and A. C. Dillon, *Phys. Rev. B: Condens. Matter Mater. Phys.*, 2011, **83**, 035406.
30 B. Ao, Z. Zhang, T. Tang and Y. Zhao, *Chem. Phys. Lett.*, 2014, **591**, 185–188.
31 Z. X. Bo and P. B. Scott, *2D Materials*, 2016, **3**, 031003.
32 S. K. Das, A. Bedar, A. Kannan and K. Jasuja, *Sci. Rep.*, 2015, **5**, 10522.
33 J. Mendham, R. C. Denney, J. D. Barnes, M. J. K. Thomas and B. Sivasankar, *Vogel's Textbook of Qualitative Chemical Analysis Sixth Edition*, Pearson Education, New Delhi, 2009.
34 P. Lambin, *Appl. Sci.*, 2014, **4**, 282.
35 S. Deng and V. Berry, *Mater. Today*, 2016, **19**, 197–212.
36 L. Niu, J. N. Coleman, H. Zhang, H. Shin, M. Chhowalla and Z. Zheng, *Small*, 2016, **12**, 272–293.
37 T. A. Prikhna, arXiv:0912.4906, 2009.
38 H. Y. Zhai, H. M. Christen, L. Zhang, M. Paranthaman, P. H. Fleming and D. H. Lowndes, *Supercond. Sci. Technol.*, 2001, **14**, 425.
39 D. Hanlon, C. Backes, E. Doherty, C. S. Cucinotta, N. C. Berner, C. Boland, K. Lee, A. Harvey, P. Lynch, Z. Gholamvand, S. Zhang, K. Wang, G. Moynihan, A. Pokle, Q. M. Ramasse, N. McEvoy, W. J. Blau, J. Wang, G. Abellan, F. Hauke, A. Hirsch, S. Sanvito, D. D. O/'Regan, G. S. Duesberg, V. Nicolosi and J. N. Coleman, *Nat. Commun.*, 2015, **6**, 8563.
40 Z. Niu, J. Chen, H. H. Hng, J. Ma and X. Chen, *Adv. Mater.*, 2012, **24**, 4144–4150.
41 L. Jiang and Z. Fan, *Nanoscale*, 2014, **6**, 1922–1945.
42 P. Broadhead and G. A. Newman, *Spectrochim. Acta, Part A*, 1972, **28**, 1915–1923.
43 P. Larkin, *Infrared and Raman Spectroscopy; Principles and Spectral Interpretation*, Elsevier Science, 2011.
44 G. Socrates, *Infrared and Raman Characteristic Group Frequencies: Tables and Charts*, Wiley, 2004.
45 D. Peak, G. W. Luther and D. L. Sparks, *Geochim. Cosmochim. Acta*, 2003, **67**, 2551–2560.
46 K. Nakamoto, *Infrared and Raman Spectra of Inorganic and Coordination Compounds, Theory and Applications in Inorganic Chemistry*, Wiley, 2008.
47 D. K. Aswal, K. P. Muthe, A. Singh, S. Sen, K. Shah, L. C. Gupta, S. K. Gupta and V. C. Sahni, *Phys. C*, 2001, **363**, 208–214.
48 W. Shin, S. Calder, O. Ugurlu and S. Girshick, *J. Nanopart. Res.*, 2011, **13**, 7187–7191.
49 C. Pistidda, S. Garroni, F. Dolci, E. G. Bardají, A. Khandelwal, P. Nolis, M. Dornheim, R. Gosalawit, T. Jensen, Y. Cerenius, S. Suriñach, M. D. Baró, W. Lohstroh and M. Fichtner, *J. Alloys Compd.*, 2010, **508**, 212–215.
50 S. Gupta, I. Z. Hlova, T. Kobayashi, R. V. Denys, F. Chen, I. Y. Zavaliy, M. Pruski and V. K. Pecharsky, *Chem. Commun.*, 2013, **49**, 828–830.
51 H. T. Tsou and W. Kowbel, *Surf. Coat. Technol.*, 1996, **79**, 139–150.
52 Y. Jia, S. Gao, Y. Jing, Y. Zhou and S. Xia, *Chem. Pap.*, 2001, **55**, 162–166.
53 J. A. Alarco, A. Chou, P. C. Talbot and I. D. R. Mackinnon, *Phys. Chem. Chem. Phys.*, 2014, **16**, 24443–24456.
54 K. A. Yates, G. Burnell, N. A. Stelmashenko, D. J. Kang, H. N. Lee, B. Oh and M. G. Blamire, *Phys. Rev. B: Condens. Matter Mater. Phys.*, 2003, **68**, 220512.
55 A. Bateni, E. Erdem, S. Repp, S. Acar, I. Kokal, W. Häßler, S. Weber and M. Somer, *J. Appl. Phys.*, 2015, **117**, 153905.
56 J. F. Moulder and J. Chastain, *Handbook of X-ray Photoelectron Spectroscopy: A Reference Book of Standard Spectra for Identification and Interpretation of XPS Data*, Physical Electronics Division, Perkin-Elmer Corporation, 1992.
57 A. Talapatra, S. K. Bandyopadhyay, P. Sen, P. Barat, S. Mukherjee and M. Mukherjee, *Phys. C*, 2005, **419**, 141–147.
58 R. P. Vasquez, C. U. Jung, M.-S. Park, H.-J. Kim, J. Y. Kim and S.-I. Lee, *Phys. Rev. B: Condens. Matter Mater. Phys.*, 2001, **64**, 052510.
59 T. A. Callcott, L. Lin, G. T. Woods, G. P. Zhang, J. R. Thompson, M. Paranthaman and D. L. Ederer, *Phys. Rev. B: Condens. Matter Mater. Phys.*, 2001, **64**, 132504.
60 Y. N. Bekish, T. V. Gaevskaya, L. S. Tsybulskaya, G.-Y. Lee and M. Kim, *Prot. Met. Phys. Chem. Surf.*, 2010, **46**, 325–331.

61 L. Li, L. H. Li, Y. Chen, X. J. Dai, T. Xing, M. Petravic and X. Liu, *Nanoscale Res. Lett.*, 2012, **7**, 417.
62 M. M. Ennaceur and B. Terreault, *J. Nucl. Mater.*, 2000, **280**, 33–38.
63 K. B. Garg, T. Chatterji, S. Dalela, M. Heinonnen, J. Leiro, B. Dalela and R. K. Singhal, *Solid State Commun.*, 2004, **131**, 343–347.
64 T. Daeneke, R. M. Clark, B. J. Carey, J. Z. Ou, B. Weber, M. S. Fuhrer, M. Bhaskaran and K. Kalantar-zadeh, *Nanoscale*, 2016, **8**, 15252–15261.
65 C. Zhao, H. Zhang, W. Si and H. Wu, *Nat. Commun.*, 2016, **7**, 12543.
66 D. T. Sawyer and P. J. Paulsen, *J. Am. Chem. Soc.*, 1958, **80**, 1597–1600.
67 D. T. Sawyer and P. J. Paulsen, *J. Am. Chem. Soc.*, 1959, **81**, 816–820.
68 G. Bester and M. Fähnle, *Phys. Rev. B: Condens. Matter Mater. Phys.*, 2005, **72**, 094102.
69 C. C. Ou, *US Pat.*, 5102464 A, 1992.
70 L. H. Rude, T. K. Nielsen, D. B. Ravnsbæk, U. Bösenberg, M. B. Ley, B. Richter, L. M. Arnbjerg, M. Dornheim, Y. Filinchuk, F. Besenbacher and T. R. Jensen, *Phys. Status Solidi A*, 2011, **208**, 1754–1773.
71 Y. Xie, Y. Dall'Agnese, M. Naguib, Y. Gogotsi, M. W. Barsoum, H. L. Zhuang and P. R. C. Kent, *ACS Nano*, 2014, **8**, 9606–9615.